DOI: https://doi.org/10.57233/ijsgs.v11i1.783

ISSNp: 2488-9229; ISSNe: 3027-1118

IJSGS FUGUSAU VOL.11(1) WEBSITE: https://fugus-ijsgs.com.ng

INTERNATIONAL JOURNAL OF SCIENCE FOR GLOBAL SUSTAINABILITY

(A PUBLICATION OF FACULTY OF SCIENCE, FEDERAL UNIVERSITY GUSAU, NIGERIA)

An Analytical Solution for the Steady-State Free Convection Flow of a Nanofluid in a Vertical Channel

M. N. Sarki[1] and Abdullahi Buhari[2]

[1]Department of Mathematics, Kebbi State University of Science and Technology Aliero

[2] Department of Mathematics, Federal University Birnin Kebbi

Corresponding Author's Email: abdullahi.buhari@fubk.edu.ng

Received on: January, 2025 **Revised and Accepted on:** February, 2025 **Published on:** March, 2025

ABSTRACT

This research analysed the steady-state free convection flow of a nanofluid in a vertical channel analytically. The nanofluid model used here include the effects of Brownian diffusion and thermophoresis. The solutions for the velocity, temperature and nanoparticle concentration profiles were obtained analytically using separation of variables and integral techniques. Nusselt and Sherwood numbers at the left wall of the channel were determined and discussed in detail. It is observed that the velocity decreases at the hot wall and increases at the cold wall due to increasing Prandtl number parameter. The same behaviour is noticed in the case of the buoyancy ratio, Grashof number, thermophoresis, and Brownian motion parameters. Furthermore, a numerical solution is also obtained and compared with the analytical solution.

Keywords: steady-state, free convection, flow, nanofluid, vertical channel

NOMENCLATURE

$C_i, i = 1-7$ = constats
c = nanofluid specific heat
T = nanofluid temperature
$\boldsymbol{q}$ = energy flux
v = nanofluid velocity
c_p = nanoparticle specific heat
D_B = Brownian diffusion coefficient
ρ_p = mass density of the nanoparticles
D_T = thermal diffusion coefficient
$\nabla\emptyset$ = gradient of $\emptyset$
T_0 = reference temperature
C_0
= reference nanoparticle volume fraction concentration
ρ_f = fluid density
$(\rho c)_f$ = heat capacity of fluid
$(\rho c)_p$
= effective heat capacity of nanoparticle material
Gr = Grashoff Number
Nt = Thermophoresis parameter Number
Nb = Brownian motion Number
Nu = Nusselt Number
pr = Prandtl Number
p = Pressure
u,v = velocity components in the x and y directions
x, y = cartesian coordinates

GREEK SYMBOLS

α = pressure gradient
β = thermal expansion coefficient
ρ = density
μ = dynamic viscosity
v = kinematic viscosity
θ = dimensionless temperature
$\emptyset$ = rescaled nanoparticle volume fraction

1.0 INTRODUCTION

When it comes to heat transfer, fluids like: water, ethylene glycol, and engine oil are commonly used, but they have a major drawback: their low thermal conductivity limits how effectively they can transfer heat. Solids, however, tend to conduct heat much better. This realization sparked interest in using solid particles at the nanoscale, leading to the development of nanofluids—a mix of tiny nanoparticles (1–100 nm) suspended in a base fluid. The term "nanofluid" was first introduced by Choi (1995) to describe these specially designed colloids. Buongiorno (2006) took a closer look at how heat moves in nanofluids, identifying seven mechanisms that could cause nanoparticles to move differently from the base fluid: inertia, Brownian diffusion, thermophoresis, diffusiophoresis, Magnus effect, fluid drainage, and gravity. Out of these, Brownian diffusion and thermophoresis turned out to be the most important.

DOI: https://doi.org/10.57233/ijsgs.v11i1.783 ISSNp: 2488-9229; ISSNe: 3027-1118
IJSGS FUGUSAU VOL.11(1) WEBSITE: https://fugus-ijsgs.com.ng

Buongiorno created a model to explain how mass, momentum, thermal energy, and nanoparticle concentration behave in nanofluids, factoring in the effects of Brownian diffusion and thermophoresis. He found that the improved heat transfer in nanofluids comes from reduced fluid viscosity, which is caused by large temperature differences within the boundary layer.

Grosan and Pop (2012) studied fully developed mixed convection flow in a vertical channel filled with a nanofluid, using the Buongiorno model to analyze the effects of Brownian motion and thermophoresis. They provided analytical solutions for velocity, temperature, and nanoparticle concentration profiles, finding that parameters like the Grashof number (Gr), Reynolds number (Re), buoyancy-ratio (Nr), Brownian motion (Nb), and thermophoresis (Nt) significantly impact flow and heat transfer. Specifically, the Nusselt number decreases with higher Nb and Nt, while the Sherwood number decreases with Nb but increases with Nt. Mostafazadeh *et al*. (2019) studied the effects of radiation on laminar natural convection of nanofluid in a vertical channel with single- and two-phase approach. Umavathi and Sheremet (2020) investigated the heat transfer of viscous fluid in a vertical channel sandwiched between nanofluid porous zones.

Shobha and Patil (2021) studied the fully developed mixed convection in a vertical channel filled with nanofluids with heat source or sink in which effects of Brownian motion coefficient, thermophoresis coefficient and heat source or sink parameter were analysed graphically. Mirzaei *et al*. (2024) investigated natural convection in a square wavy porous cavity subjected to a partial magnetic field, using numerical simulations to analyze the effects of key parameters such as magnetic field length, Rayleigh number (Ra), Hartmann number (Ha), Darcy number (Da), and wave number of wall on fluid flow and heat transfer.

Sani, and Kaita (2023) investigated steady-state free convection in a vertical channel with heat and mass transfer, under the influence of a uniform magnetic field and temperature-dependent thermal conductivity. They focused on the effects of variable thermal conductivity, magnetic fields, and buoyancy forces on fluid flow and heat transfer. Puspitasari et al. (2024) investigates steady natural convection from a vertical hot plate with variable radiation and constant heat flux and focuses on understanding the velocity and temperature distribution characteristics in the boundary layer over the plate.

Ratha et al. (2022) investigates the two-dimensional unsteady flow of a Casson nanofluid over a shrinking horizontal sheet under the influence of an inclined magnetic field and Joule heating. They analysed the effects of various parameters, such as magnetic field inclination, unsteadiness, thermal buoyancy, and chemical reaction, on the velocity, temperature, and concentration profiles of the nanofluid. Ahmad et al. (2020) investigated the analytical solutions for free convection flow of Casson nanofluid over an infinite vertical plate. Jha and Sarki (2019) studied Chemical reaction and Dufour effects on nonlinear free convection heat and mass transfer flow near a vertical moving porous plate. Umar et al (2024) studied the free convective MHD flow of Jeffrey fluid in a porous medium in the presence of heat source/sink and the influence of different parameters such as: thermal Grashof number, mass Grashof number, Jeffrey parameter and heat source/sink, Peclet number for heat and mass transfer (Pe and Pem), and radiation parameter were investigated. Sarki and Garba (2024) investigated the impact of heat source/sink on non-linear free convection fluid flow with chemical reaction. Ajibade and Umar (2020) studied mixed convection flow in a vertical channel in the presence of wall conduction, variable thermal conductivity and viscosity. Yale et al. (2024) investigated mixed convection flow of heat generating/absorbing fluid in a vertical channel with asymmetric heating condition.

The objective of the present study is to investigate the analytical solution of steady-state free convection flow of a nanofluid in a vertical channel using the model proposed by Buongiorno (2006). Both walls of the channel are kept at constant temperatures and concentrations. The effects of free convection, buoyancy-ratio, Brownian motion, and thermophoretic parameters are discussed about temperature and velocity distributions in the channel. To the best of our knowledge, this problem has not been studied before.

2.0 MATHEMATICAL ANALYSIS

Consider a nanofluid that steadily flows between two vertical and parallel plane walls. The distance between the walls is L. We select a coordinate system in which the $x-$axis is aligned parallel to the gravitational acceleration vector $\boldsymbol{g}$, but with the opposite direction. The $y-$axis is orthogonal to the channel walls, and the origin of the axes is such that the positions of the channel walls are $y = 0$ and $y = L$, respectively. It is assumed that the temperature and nanoparticles concentration at the wall at $y = 0$ are T_1 and C_1, while the temperature and nanoparticles concentration at the wall at $y = L$ are T_2 and C_2, respectively. It is also assumed that the value of velocity at the channel entrance is u_0.

DOI: https://doi.org/10.57233/ijsgs.v11i1.783 ISSNp: 2488-9229; ISSNe: 3027-1118
IJSGS FUGUSAU VOL.11(1) WEBSITE: https://fugus-ijsgs.com.ng

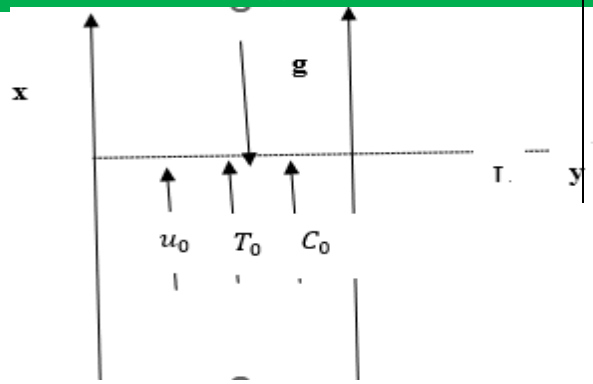

Figure 1. Physical Configuration of the Flow

Assuming the Oberbec-Boussinesq approximation, the following four field equations embody the conservation of total mass, momentum, thermal energy, and nanoparticle concentration in vectorial form as:

$$\nabla \cdot v = 0 \tag{1}$$

$$\rho_f(v \cdot \nabla v) = -\nabla p + \mu\nabla^2 v + \{C\rho_p + (1-C)[\rho_f(1-\beta(T-T_0))]\}\boldsymbol{g} \tag{2}$$

$$(\rho c)_f(v \cdot \nabla T) = k\nabla^2 T + (\rho c)_p\left[D_B \nabla T \cdot \nabla C + \left(\frac{D_T}{T_0}\right)\nabla T \cdot \nabla T\right] \tag{3}$$

$$v \cdot \nabla C = D_B \nabla^2 C + \left(\frac{D_T}{T_0}\right)\nabla^2 T \tag{4}$$

Linearizing the momentum equation (2), with assumption that the nanoparticle concentration is dilute and reference pressure of suitable choice, it can be written as:

$$\rho_f(v \cdot \nabla v) = -\nabla p + \mu\nabla^2 v + [(\rho_p - \rho_{f0})(C - C_0) - (1 - C_0)\rho_{f0}\beta(T - T_0)]\boldsymbol{g} \tag{5}$$

The fluid velocity is assumed to be parallel to the x axis, so that only x component u of velocity v does not vanish. If the fully developed assumption is adopted (say, far from the channel's entrance), the following relations apply:

$$\left.\begin{aligned} v = 0, \quad \frac{\partial u}{\partial x} = 0, \quad \frac{\partial T}{\partial x} = 0, \quad \frac{\partial C}{\partial x} = 0 \\ \frac{\partial p}{\partial y} = 0, \quad \frac{\partial p}{\partial x} = \frac{dp}{dx} = constant \end{aligned}\right\} \tag{6}$$

Then equations (1), (2), (3) and (4) become:

$$-\frac{dp}{dx} + \mu\frac{d^2u}{dy^2} + [(1 - C_0)\rho_{fo}\beta(T - T_0) - (\rho_f - \rho_{f0})(C - C_0)]g = 0 \tag{7}$$

$$k\frac{d^2T}{dy^2} + (\rho c)_p\left[D_B\frac{dC}{dy}\frac{dT}{dy} + \left(\frac{D_T}{T_0}\right)\left(\frac{dT}{dy}\right)^2\right] = 0 \tag{8}$$

$$D_B\frac{d^2C}{dy^2} + \left(\frac{D_T}{T_0}\right)\frac{d^2T}{dy^2} = 0 \tag{9}$$

And are subjected to the boundary conditions

$$\left.\begin{aligned} u = 0, \quad T = T_1, \quad C = C_1 \quad \text{at } y = 0 \\ u = 0, \quad T = T_2, \quad C = C_2 \quad \text{at } y = L \end{aligned}\right\} \tag{10}$$

Introducing the following dimensionless variables

$$\left.\begin{aligned} Y = \frac{y}{L}, \quad U(Y) = \frac{u(y)}{u_0}, \quad P(Y) = \frac{p(y)}{\rho u_0^2} \\ \theta(Y) = \frac{(T - T_0)}{(T_2 - T_0)}, \quad \emptyset(Y) = \frac{(C - C_0)}{(C_2 - C_0)} \end{aligned}\right\} \tag{11}$$

To determine pressure gradient from equation (5), the mass flux conservation Q is required

$$\int_0^L u(y)dy = Q \tag{12}$$

Using equation (11) into (5), we have:

$$\frac{d^2u}{dy^2} = \frac{u_0^2}{L^2}\frac{d^2U}{dY^2} \tag{13}$$

Substituting (13) into (5), we get

$$-\frac{dp}{dx} + \mu\frac{d^2u}{dy^2} + [(1 - C_0)\rho_{fo}\beta(T - T_0) - (\rho_f - \rho_{f0})(C - C_0)]g = 0$$

DOI: https://doi.org/10.57233/ijsgs.v11i1.783 ISSNp: 2488-9229; ISSNe: 3027-1118
IJSGS FUGUSAU VOL.11(1) WEBSITE: https://fugus-ijsgs.com.ng

$$\mu\frac{d^2u}{dy^2}+\left[(1-C_0)\rho_{fo}\beta(T-T_0)-(\rho_f-\rho_{f0})(C-C_0)\right]g+\alpha=0$$

$$\mu\frac{u_0^2}{L^2}\frac{d^2U}{dY^2}+\left[(1-C_0)\rho_{fo}\beta(T-T_0)-(\rho_f-\rho_{f0})(C-C_0)\right]g+\alpha=0$$

$$\mu\frac{u_0^2}{L^2}\frac{d^2U}{dY^2}+\left[(1-C_0)\rho_{fo}\beta(T-T_0)\frac{(T_2-T_0)}{(T_2-T_0)}-(\rho_f-\rho_{f0})(C-C_0)\frac{(C_2-C_0)}{(C_2-C_0)}\right]g+\alpha=0$$

$$\frac{\mu u_0^2}{L^2\rho_{fo}}\frac{d^2U}{dY^2}+(1-C_0)\beta g(T-T_0)\frac{(T_2-T_0)}{(T_2-T_0)}-(\rho_f-\rho_{f0})(C-C_0)\frac{(C_2-C_0)}{(C_2-C_0)}g+\alpha=0$$

$$\frac{\mu u_0^2}{L^2\rho_{fo}}\frac{d^2U}{dY^2}+(1-C_0)g\beta(T_2-T_0)\frac{(T-T_0)}{(T_2-T_0)}-g(\rho_f-\rho_{f0})(C_2-C_0)\frac{(C-C_0)}{(C_2-C_0)}+\alpha=0$$

$$\frac{d^2U}{dY^2}+\frac{L^2\rho_{fo}}{\mu u_0^2}(1-C_0)g\beta(T_2-T_0)\frac{(T-T_0)}{(T_2-T_0)}-\frac{L^2\rho_{fo}}{\mu u_0^2}g(\rho_f-\rho_{f0})(C_2-C_0)\frac{(C-C_0)}{(C_2-C_0)}+\alpha=0$$

$$\frac{d^2U}{dY^2}+Gr\theta(Y)-Nr\emptyset(Y)+\alpha=0 \qquad (14)$$

Equation (14) is Momentum equation. And using equation (11) into (9)

$$\frac{dT}{dy}=\frac{dT}{dY}\cdot\frac{dY}{dy}$$

$$=\frac{(T_2-T_0)}{L}\frac{d\theta}{dY}$$

$$\frac{d^2T}{dy^2}=\frac{(T_2-T_0)^2}{L^2}\frac{d^2\theta}{dY^2} \qquad (15)$$

$$\frac{dC}{dy}=\frac{dC}{dY}\cdot\frac{dY}{dy}$$

$$=\frac{(C_2-C_0)}{L}\frac{d\emptyset}{dY}$$

$$\frac{d^2C}{dy^2}=\frac{(C_2-C_0)^2}{L^2}\frac{d^2\emptyset}{dY^2} \qquad (16)$$

Substituting (15) and (16) into

$$k\frac{d^2T}{dy^2}+(\rho c)_p\left[D_B\frac{dC}{dy}\frac{dT}{dy}+\left(\frac{D_T}{T_0}\right)\left(\frac{dT}{dy}\right)^2\right]=0$$

$$\frac{k}{(\rho c)_p}\frac{d^2T}{dy^2}+\left[D_B\frac{dC}{dy}\frac{dT}{dy}+\left(\frac{D_T}{T_0}\right)\left(\frac{dT}{dy}\right)^2\right]=0$$

$$\frac{k}{(\rho c)_p}\frac{d^2T}{dy^2}+D_B\frac{dC}{dy}\frac{dT}{dy}+\left(\frac{D_T}{T_0}\right)\left(\frac{dT}{dy}\right)^2=0$$

$$\frac{k}{(\rho c)_p}\frac{(T_2-T_0)^2}{L^2}\frac{d^2\theta}{dY^2}+D_B\frac{(C_2-C_0)}{L}\frac{d\emptyset}{dY}\frac{(T_2-T_0)}{L}\frac{d\theta}{dY}+\left(\frac{D_T}{T_0}\right)\left(\frac{(T_2-T_0)}{L}\frac{d\theta}{dY}\right)^2=0$$

$$\frac{k}{(\rho c)_p}\frac{(T_2-T_0)^2}{L^2}\frac{d^2\theta}{dY^2}+D_B\frac{(C_2-C_0)(T_2-T_0)}{L^2}\frac{d\emptyset}{dY}\frac{d\theta}{dY}+\left(\frac{D_T}{T_0}\right)\frac{(T_2-T_0)^2}{L^2}\left(\frac{d\theta}{dY}\right)^2=0$$

$$\frac{k}{(\rho c)_p}\frac{d^2\theta}{dY^2}+D_B\frac{(C_2-C_0)}{(T_2-T_0)}\frac{d\emptyset}{dY}\frac{d\theta}{dY}+\left(\frac{D_T}{T_0}\right)\left(\frac{d\theta}{dY}\right)^2=0$$

$$\frac{k}{(\rho c)_p}\frac{d^2\theta}{dY^2}+D_B(C_2-C_0)\frac{d\emptyset}{dY}\frac{d\theta}{dY}+\left(\frac{D_T}{T_0}\right)(T_2-T_0)\left(\frac{d\theta}{dY}\right)^2=0$$

$$\frac{d^2\theta}{dY^2}+D_B\frac{(C_2-C_0)}{\frac{k}{(\rho c)_p}}\frac{d\emptyset}{dY}\frac{d\theta}{dY}+\left(\frac{D_T}{T_0}\right)\frac{(T_2-T_0)}{\frac{k}{(\rho c)_p}}\left(\frac{d\theta}{dY}\right)^2=0$$

$$\frac{d^2\theta}{dY^2}+\frac{D_B(C_2-C_0)}{\frac{k}{(\rho c)_p}}\frac{d\emptyset}{dY}\frac{d\theta}{dY}+\frac{D_T(T_2-T_0)}{T_0\frac{k}{(\rho c)_p}}\left(\frac{d\theta}{dY}\right)^2=0$$

$$\frac{d^2\theta}{dY^2}+Pr\left[Nb\frac{d\emptyset}{dY}\frac{d\theta}{dY}+Nt\left(\frac{d\theta}{dY}\right)^2\right]=0 \qquad (17)$$

Equation (17) is Energy equation. Also using equation (11) into (8)

$$D_B\frac{d^2C}{dy^2}+\left(\frac{D_T}{T_0}\right)\frac{d^2T}{dy^2}=0$$

DOI: https://doi.org/10.57233/ijsgs.v11i1.783 ISSNp: 2488-9229; ISSNe: 3027-1118

IJSGS FUGUSAU VOL.11(1) WEBSITE: https://fugus-ijsgs.com.ng

$$D_B\frac{(C_2-C_0)^2}{L^2}\frac{d^2\emptyset}{dY^2}+\left(\frac{D_T}{T_0}\right)\frac{(T_2-T_0)^2}{L^2}\frac{d^2\theta}{dY^2}=0$$

$$D_B\frac{(C_2-C_0)^2}{L^2}\frac{L^2}{(C_2-C_0)(T_2-T_0)}\frac{d^2\emptyset}{dY^2}+\left(\frac{D_T}{T_0}\right)\frac{(T_2-T_0)^2}{L^2}\frac{L^2}{(C_2-C_0)(T_2-T_0)}\frac{d^2\theta}{dY^2}=0$$

$$D_B\frac{(C_2-C_0)}{(T_2-T_0)}\frac{d^2\emptyset}{dY^2}+\left(\frac{D_T}{T_0}\right)\frac{(T_2-T_0)}{(C_2-C_0)}\frac{d^2\theta}{dY^2}=0$$

$$\frac{d^2\emptyset}{dY^2}+\frac{\left(\frac{D_T}{T_0}\right)(T_2-T_0)^2}{D_B(C_2-C_0)^2}\frac{d^2\theta}{dY^2}=0$$

$$\frac{d^2\emptyset}{dY^2}+\frac{Nt}{Nb}\frac{d^2\theta}{dY^2}=0 \qquad (18)$$

Equation (18) is Concentration equation. And the boundary conditions equation (27) become:

$$\left.\begin{array}{lll} U(0)=0, & \emptyset(0)=-1, & \theta(0)=-1 \\ U(1)=0, & \emptyset(1)=1, & \theta(1)=1 \end{array}\right\} \qquad (19)$$

where α is the pressure gradient, Gr is the Grashoff number, Re is the Reynolds number, Pr is the Prandtl number, Nr is the buoyancy ratio parameter, Nb is the Brownian motion parameter and Nt is the thermophoresis parameter. The parameters are given by:

$$\left.\begin{array}{c} \alpha=-\frac{dP}{dY}, \qquad Gr=\frac{(1-C_0)g\beta(T_2-T_0)}{v^2}L^3, \\ Re=\frac{u_0L}{v}, \qquad Pr=\frac{v}{\alpha}, \qquad Nr=\frac{(\rho_p-\rho_f)g(C_2-C_0)}{\mu u_0}L^2, \\ Nb=D_B(C_2-C_0), \qquad Nt=\frac{D_T(T_2-T_0)}{T_0} \end{array}\right\} \qquad (20)$$

The physical quantities of interest are the Nusselt (Nu) number, Sherwood (Sh) number and skin friction defined as;

$$\left.\begin{array}{l} Nu=-\frac{L}{T_2-T_0}\left(\frac{\partial T}{\partial Y}\right)_{Y=0}=-\theta'(0) \\ Sh=-\frac{L}{C_2-C_0}\left(\frac{\partial C}{\partial Y}\right)_{Y=0}=-\emptyset'(0) \\ \tau_0=\frac{dU}{dY}\Big|_{Y=0} \\ \tau_1=\frac{dU}{dY}\Big|_{Y=1} \end{array}\right\} \qquad (21)$$

To find the solution of the governing equations (14), (17) and (18) concerning boundary conditions (19), we obtain:

$$\theta(Y)=C_3+C_4e^{-C_2PrY} \qquad (22)$$

$$\emptyset(Y)=-\frac{Nt}{Nb}(C_3+C_4e^{-C_2PrY})+C_1Y-\frac{C_1}{2} \qquad (23)$$

On substituting Equation (22) and (23) into Equation (14), the dimensionless fluid velocity is obtained as:

$$\begin{aligned} U(Y)=&\left(Gr+Nr\frac{Nt}{Nb}\right)\frac{C_4}{C_2^2Pr^2} \\ &+\left[\frac{C_3}{2}\left(Gr+Nr\frac{Nt}{Nb}\right)+\frac{NrC_1}{4}-\frac{NrC_1}{6}-\left(Gr+Nr\frac{Nt}{Nb}\right)\frac{C_4}{C_2^2Pr^2}+\frac{C_4}{C_2^2Pr^2}\left(Gr+Nr\frac{Nt}{Nb}\right)e^{-C_2Pr}+\frac{\alpha}{2}\right]Y \\ &+\left[-\frac{C_3}{2}\left(Gr+Nr\frac{Nt}{Nb}\right)-\frac{NrC_1}{4}-\frac{\alpha}{2}\right]Y^2-\frac{C_4}{C_2^2Pr^2}\left(Gr+Nr\frac{Nt}{Nb}\right)e^{-C_2PrY} \\ &+\frac{NrC_1}{6}Y^3 \qquad (24) \end{aligned}$$

For purely buoyancy driven flow (natural convection flow), α = 0 and Equation (24) becomes:

$$\begin{aligned} U(Y)=&\frac{C_5}{C_2^2Pr^2}+\left[\frac{C_7}{2}+\frac{C_6}{6}-\frac{C_5}{C_2^2Pr^2}+\frac{C_5}{C_2^2Pr^2}e^{-C_2Pr}\right]Y-\frac{C_7}{2}Y^2-\frac{C_6}{6}Y^3 \\ &-\frac{C_5}{C_2^2Pr^2}e^{-C_2PrY} \qquad (25) \end{aligned}$$

where $C_i, i=1-7$ are constants, given by

DOI: https://doi.org/10.57233/ijsgs.v11i1.783 ISSNp: 2488-9229; ISSNe: 3027-1118

IJSGS FUGUSAU VOL.11(1) WEBSITE: https://fugus-ijsgs.com.ng

$$C_1 = 2\left(1+\frac{Nt}{Nb}\right), \quad C_2 = NbC_1, \quad C_3 = \frac{(e^{C_2Pr}+1)}{(e^{C_2Pr}-1)}$$
$$C_4 = -\frac{2e^{C_2Pr}}{(e^{C_2Pr}-1)}, \quad C_5 = C_4\left(Gr+Nr\frac{Nt}{Nb}\right), \quad C_6 = -NrC_1,$$
$$C_7 = C_3\left(Gr+Nr\frac{Nt}{Nb}\right)+\frac{NrC_1}{2} \qquad (26)$$

Using equations (22), (23) and (26), Nusselt number and sherwood numbers are defined by;

$$Nu = -\theta'(0) = C_4C_2Pr$$
$$Sh = -\emptyset'(0) = -\left(\frac{Nt}{Nb}C_4C_2Pr + C_1\right) \qquad (27)$$

Therefore, fluid flowing against the boundary surface would experience viscous forces called skin friction. It is the fluid forces against the direction of the wall surface and is given by:

$$\tau_0 = \frac{dU}{dY}\Big|_{Y=0} = \frac{C_5}{C_2^2Pr^2}e^{-C_2Pr} - \frac{C_5}{C_2^2Pr^2} + \frac{C_5}{C_2Pr} + \frac{C_6}{6} + \frac{C_7}{2}$$
$$\tau_0 = \frac{dU}{dY}\Big|_{Y=1} = \frac{C_5}{C_2^2Pr^2}e^{-C_2Pr} - \frac{C_5}{C_2^2Pr^2} + \frac{C_5}{C_2Pr}e^{-C_2Pr} - \frac{C_6}{3} + \frac{C_7}{2} \qquad (28)$$

3.0 RESULTS AND DISCUSSION

This study examines the analytical solution of steady-state free convection of a nanofluid in a vertical channel. Additionally, a MATLAB program was developed to generate line graphs illustrating velocity $U(Y)$, temperature $\theta(Y)$, and nanoparticle concentration $\emptyset(Y)$ profiles, providing a clear visualization of the problem and showcasing the influence of some various key parameters. These parameters include the Prandtl number (Pr), Brownian motion parameter (Nb), Grashof number for heat transfer (Gr), thermophoresis parameter (Nt), and the buoyance ratio parameter (Nr). The fixed values chosen for analysis are $Pr = 0.71$, $Gr = 1000$, $Nr = Nt = Nb = 0.5$. High order finite difference method is used to compare the analytical solution and numerical solution of some governing parameters.

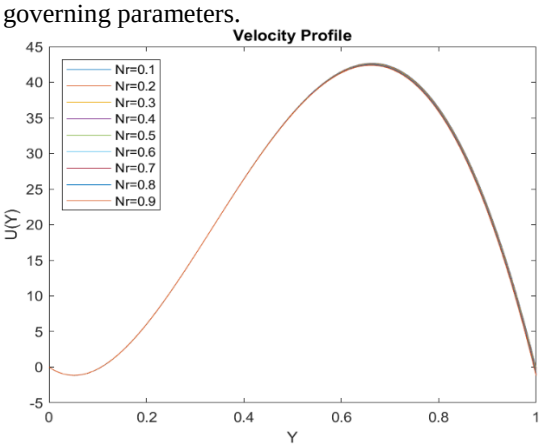

Figure 2. Variation of Dimensionless Velocity When $Nr = 0.1, 0.2, 0.3, 0.4, 0.5, 0.6, 0.7, 0.8, 0.9$, $Pr = 0.71$ and $Nt = Nb = 0.5$

Figure 2 illustrates the variation of dimensionless velocity $U(Y)$ for different values of the buoyancy ratio parameter (Nr) while keeping other parameters constant. Specifically, the figure shows how the velocity profile changes as (Nr) increases from 0.1 to 0.9, with fixed values of the Prandtl number $(Pr = 0.71)$ and the Brownian motion and thermophoresis parameters $(Nb = Nt = 0.5)$. Near the hot wall $(Y = 0)$, the velocity decreases as Nr increases and near the cold wall $(Y = 1)$ the velocity increases as Nr increases. Increasing Nr leads to a deceleration of the flow near the hot wall and an acceleration near the cold wall.

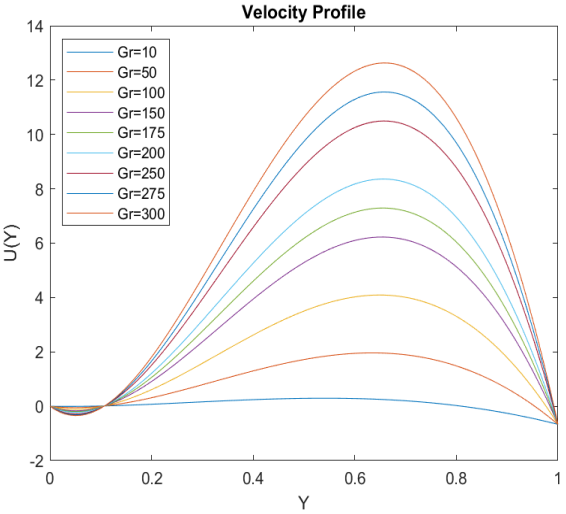

Figure 3. Variation of Dimensionless Velocity When $Gr = 10, 50, 100, 150, 175, 200, 250, 275, 300$, $Pr = 0.71$, $Nr = Nt = Nb = 0.5$

Figure 3 demonstrates the variation of dimensionless velocity $U(Y)$ across the vertical channel for different values of the Grashoff number Gr. The Grashoff number is a dimensionless parameter that represents the ratio of buoyancy forces to viscous forces in a fluid. It is a key parameter in free convection problems, as it indicates the strength of the buoyancy-driven flow. The figure shows how the velocity profile $U(Y)$ changes as

DOI: https://doi.org/10.57233/ijsgs.v11i1.783

ISSNp: 2488-9229; ISSNe: 3027-1118

IJSGS FUGUSAU VOL.11(1)

WEBSITE: https://fugus-ijsgs.com.ng

the Grashoff number Gr increases and as Gr increases, the velocity near the hot wall (left wall, $Y = 0$) decreases, while the velocity near the cold wall (right wall, $Y = 1$) increases.

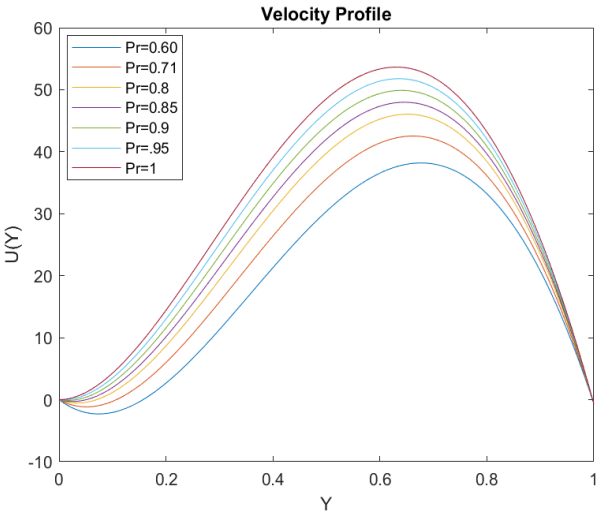

Figure 4. Variation of Dimensionless Velocity When $Pr = 0.60, 0.71, 0.8, 0.85, 0.9, 0.95, 1$ and $Nr = Nt = Nb = 0.5$

Figure 4 shows the variation of dimensionless velocity $(U(Y))$ for different values of the Prandtl number (Pr) while keeping other parameters constant. Specifically, the figure shows how the velocity profile changes as Pr increases from $0.6\ to\ 1$, with fixed values of the Brownian motion and thermophoresis parameters $(Nr = Nb = Nt = 0.5)$. Near the hot wall $(Y = 0)$, the velocity decreases as Pr increases and near the cold wall $(Y = 1)$, the velocity increases as Pr increases.

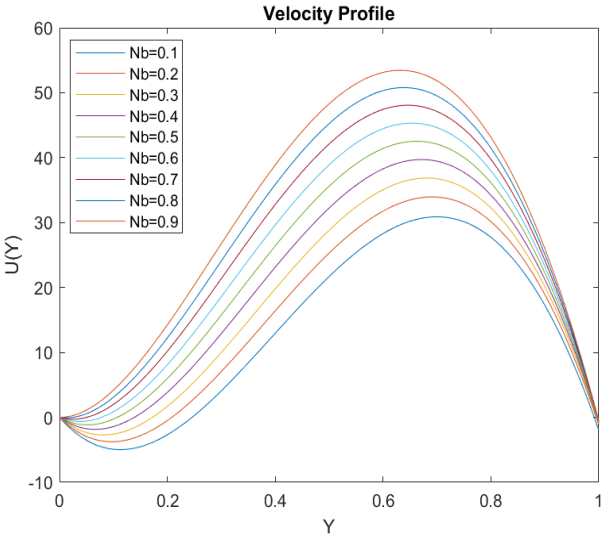

Figure 5. Variation of Dimensionless Velocity When $Nb = 0.1, 0.2, 0.3, 0.4, 0.5, 0.6, 0.7, 0.8, 0.9$, $Nr = Nt = 0.5$ and $Pr = 0.71$

Figure 5 illustrates the variation of dimensionless velocity $U(Y)$ for different values of the Brownian motion parameter (Nb), while keeping other parameters constant. Specifically, the figure shows how the velocity profile changes as Nb increases from $0.1\ to\ 0.8$, with fixed values of the buoyancy ratio parameter $(Nr = 0.5)$, thermophoresis parameter $(Nt = 0.5)$, and Prandtl number $(Pr = 0.71)$. Near the hot wall $(Y = 0)$, the velocity decreases as Nb increases and near the cold wall $(Y = 1)$, the velocity increases as Nb increases.

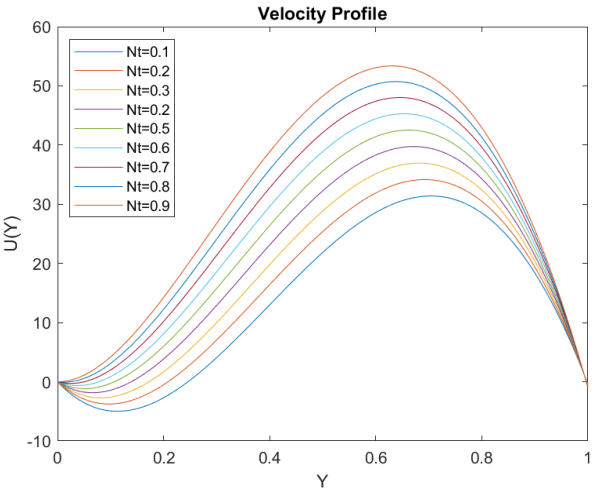

Figure 6. Variation of Dimensionless Velocity When $Nt = 0.1, 0.2, 0.3, 0.4, 0.5, 0.6, 0.7, 0.8, 0.9$, $Nr = Nb = 0.5$ and $Pr = 0.71$

Figure 6 demonstrates the variation of dimensionless velocity $U(Y)$ for different values of the thermophoresis parameter (Nt), while keeping other parameters constant. Specifically, the figure shows how the velocity profile changes as Nt increases from $0.1\ to\ 0.9$, with fixed values of the buoyancy ratio parameter $(Nr = 0.5)$, Brownian motion parameter $(Nb = 0.5)$, and Prandtl number $(Pr = 0.71)$. Near the hot wall $(Y = 0)$, the velocity decreases as Nt increases and near the cold wall $(Y = 1)$, the velocity increases as Nt increases.

DOI: https://doi.org/10.57233/ijsgs.v11i1.783

ISSNp: 2488-9229; ISSNe: 3027-1118

IJSGS FUGUSAU VOL.11(1)

WEBSITE: https://fugus-ijsgs.com.ng

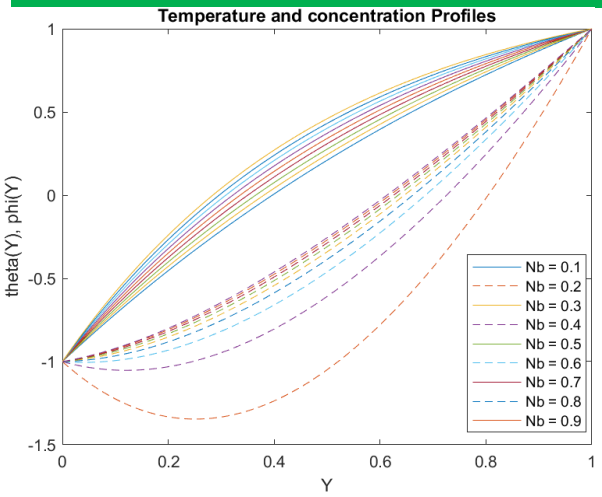

Figure 7. Variation of Dimensionless Temperature (Full Line) and Dimensionless Concentration (Broken Line) When $Nb = 0.1, 0.2, 0.3, 0.4, 0.5, 0.6, 0.7, 0.8, 0.9$, $Nr = 100$, $Nt = 0.5$ and $Pr = 0.71$

Figure 7 illustrates the variation of dimensionless temperature $\theta(Y)$ and dimensionless nanoparticle concentration $\emptyset(Y)$ profiles for different values of the Brownian motion parameter (Nb), while keeping other parameters constant. Specifically, the figure shows how the temperature and concentration profiles change as Nb increases from $0.1\ to\ 0.9$, with fixed values of the buoyancy ratio parameter $(Nr = 0.5)$, thermophoresis parameter $(Nt = 0.5)$, and Prandtl number $(Pr = 0.71)$. As Nb increases, the temperature profile increases across the channel and as Nb increases, the nanoparticle concentration profile also increases across the channel. The concentration of nanoparticles is higher near the cold wall $(Y = 1)$ compared to the hot wall $(Y = 0)$, reflecting the tendency of nanoparticles to move from the hot wall to the cold wall due to thermophoresis.

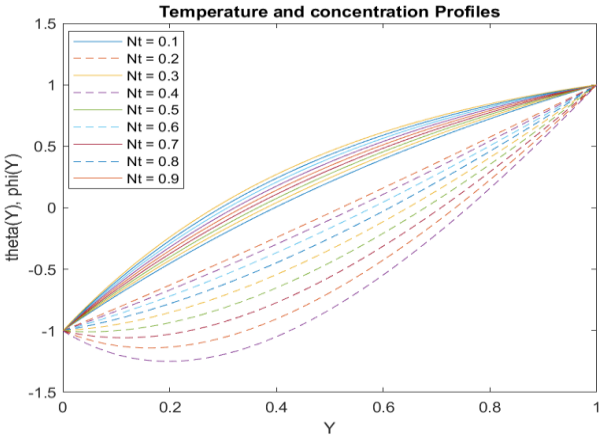

Figure 8. Variation of Dimensionless Temperature (Full Line) and Dimensionless Concentration (Broken Line) when $Nt = 0.1, 0.2, 0.3, 0.4, 0.5, 0.6, 0.7, 0.8, 0.9$, $Nr = Nb = 0.5$ and $Pr = 0.71$

Figure 8 shows the variation of dimensionless temperature $\theta(Y)$ and dimensionless nanoparticle concentration $\emptyset(Y)$ profiles for different values of the thermophoresis parameter (Nt), while keeping other parameters constant. Specifically, the figure shows how the temperature and concentration profiles change as Nt increases from $1\ to\ 5$, with fixed values of the buoyancy ratio parameter $(Nr = 0.5)$, Brownian motion parameter $(Nb = 0.5)$, and Prandtl number $(Pr = 0.71)$. As Nt increases, the temperature profile increases across the channel and as Nt increases, the nanoparticle concentration profile decreases across the channel. A higher Nt means that the nanoparticles are more strongly driven from the hot wall to the cold wall, which enhances the thermal conductivity of the nanofluid.

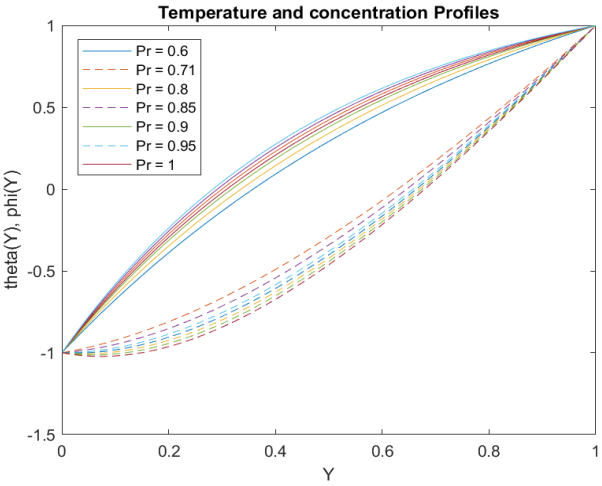

Figure 9. Variation of Dimensionless Temperature (Full Line) and Dimensionless Concentration (Broken Line) When $Pr = 0.6, 0.71, 0.8, 0.85, 0.9, 0.95, 1$, $Nr = Nb = Nt = 0.5$

Figure 9 illustrates the variation of dimensionless temperature $\theta(Y)$ and dimensionless nanoparticle concentration $\emptyset(Y)$ profiles across the vertical channel for different values of the Prandtl number Pr. The Prandtl number is a dimensionless parameter that represents the ratio of momentum diffusivity (viscosity) to thermal diffusivity. The figure shows how the temperature and nanoparticle concentration profiles change as the Prandtl number Pr increases. As Pr increases, the temperature profile $\theta(Y)$ increases across the channel and the nanoparticle concentration profile $\emptyset(Y)$ also increases with increasing Pr. The temperature profile (full line) shows that the temperature is higher near the hot wall $(Y = 0)$ and decreases towards the cold wall $(Y = 1)$ and

DOI: https://doi.org/10.57233/ijsgs.v11i1.783

ISSNp: 2488-9229; ISSNe: 3027-1118

IJSGS FUGUSAU VOL.11(1)

WEBSITE: https://fugus-ijsgs.com.ng

the nanoparticle concentration profile (broken line) shows that the concentration of nanoparticles is higher near the cold wall ($Y = 1$) compared to the hot wall ($Y = 0$).

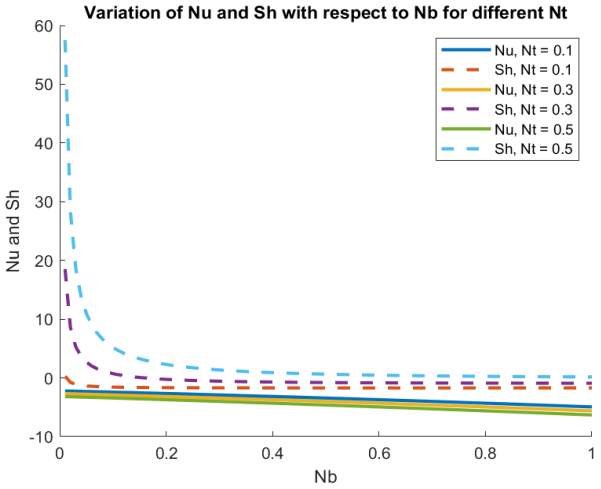

Figure 10. Variation of Nusselt Number (Nu) and Sherwood Number (Sh) With Respect To Nb, When $Nt = 0.1,\ 0.3,\ 0.5$

Figure 10 demonstrates the variation of the Nusselt number (Nu) and Sherwood number (Sh) with respect to the Brownian motion parameter (Nb), for different values of the thermophoresis parameter (Nt). Specifically, the figure shows how the Nusselt and Sherwood numbers change as Nb varies, with Nt fixed at three different values $Nt = 0.1,\ Nt = 0.3, and\ Nt = 0.5$. As Nb increases, the Nusselt number decreases and as Nb increases, the Sherwood number also decreases. A higher Nb leads to a thicker thermal boundary layer, which reduces the temperature gradient at the wall and more uniform distribution of nanoparticles throughout the fluid, reducing the concentration gradient at the wall, For a given Nb, the Nusselt and Sherwood numbers decrease as Nt increases.

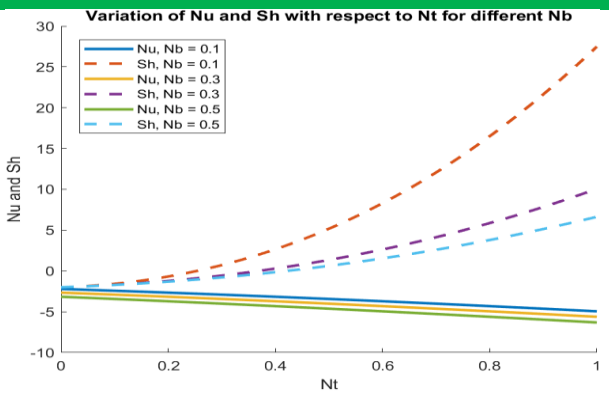

Figure 11 Variation of Nusselt Number (Nu) and Sherwood Number (Sh) With Respect To Nt When $Nb = 0.1,\ 0.3,\ 0.5$

Figure 11 illustrates the variation of the Nusselt number (Nu) and Sherwood number (Sh) with respect to the thermophoresis parameter (Nt), for different values of the Brownian motion parameter (Nb). Specifically, the figure shows how the Nusselt and Sherwood numbers change as Nt varies, with Nb fixed at three different values $Nb = 0.1,\ Nb = 0.3, and\ Nb = 0.5$. As Nt increases, the Nusselt number decreases and as Nt increases, the Sherwood number increases. A higher Nt means that the nanoparticles are more strongly driven from the hot wall to the cold wall, which enhances the thermal conductivity of the nanofluid. For a given Nt, the Nusselt number decreases as Nb increases and For a given Nt, the Sherwood number decreases as Nb increases.

It can be seen from Figs. 2– 6 that with increasing values of the buoyancy-ratio parameter Nr, the Prandtl number, the Grashof number Gr, the Brownian motion parameter, Nb, and the thermophoresis parameter, Nt, the flow decelerate near the hot wall and accelerate near the cold wall. For the considered values of the governing parameters, the magnitude of velocity is always lower than in the regular (Newtonian) fluid case. Further, Figs. 7,8 and 9 display the dimensionless temperature (full lines) and the rescaled nanoparticle volume fraction (dotted lines) profiles for different values of Nb and $Nt = 0.5$ (Fig. 7) , Nt and $Nb = 0.5$ (Fig. 8) and Pr and $Nb = Nt = 0.5$. Thus, we notice from Fig. 7 that both temperature and nanoparticle volume fraction profiles increase with the increasing of the parameter Nb, while from Fig. 8 temperature profile increases and nanoparticle volume fraction decreases with the increasing of Nt and from Fig. 9 both temperature and nanoparticle volume profiles increase with the increasing of the parameter Pr. Finally, Figs. 10 and 11 present the variation of reduced Nusselt number $-\theta'(0)$ (full line) and reduced Sherwood number $-\emptyset'(0)$

DOI: https://doi.org/10.57233/ijsgs.v11i1.783

ISSNp: 2488-9229; ISSNe: 3027-1118

IJSGS FUGUSAU VOL.11(1)

WEBSITE: https://fugus-ijsgs.com.ng

(dotted line) with respect to Nb and Nt. These figures show that the Nusselt number decreases with the increasing of Nb and Nt, while the Sherwood number decreases with the increasing of Nb and increases with the increasing of Nt, which is in agreement with the temperature and the nanoparticle volume fraction profiles shown in Figs. 6 and 7. We notice that the reduced Sherwood number is more sensitive with the variation of the parameters Nb and Nt than the reduced Nusselt number. It is worth to mention that $Eq.(14)$ is uncoupled with the system of $equations$ (17) and (18). Thus, parameters $Gr, Nr,$ and a have no influence on the Nusselt and Sherwood numbers.

Table 1: Comparison Between Analytical and Numerical Results.

					$\theta'(0)$		$\emptyset'(0)$	
Gr	Pr	Nr	Nt	Nb	*Analytic*	*Numeric*	*Analytic*	*Numeric*
0	1	0	0	0.2	2.426593	2.426593	2.00000	2.00000
		0	0.2	0.2	2.905546	2.905530	1.094454	1.094470
		5	0.2	0.2	2.905546	2.905530	1.094454	1.094470
1000	1	0	0	0.2	2.426596	2.426593	2.00000	2.00000
		0	0.2	0.2	2.905546	2.905530	1.094454	1.094470
		5	0.2	0.2	2.905546	2.905530	1.094454	1.094470

Table 1 compares the analytical and numerical results for $\theta'(0)$ and $\emptyset'(0)$ under different values of the governing parameters; $\frac{Gr}{Re}$, Nr, Nb and Nt with fixed $Pr = 1$. The analytical and numerical results are in good agreement. This indicates that Pr has a significant effect on both Nusselt and Sherwood numbers.

Table 2: The Values of $\theta'(0)$ and $\emptyset'(0)$in the Present Work and Literature Review for $Pr = 1$, $Gr = 1000$, $Re = 1$

Grosan and Pop, (2012)		Present Study		Grosan and Pop, (2012)		Present Study	
$\theta'(0)$		$\theta'(0)$		$\emptyset'(0)$		$\emptyset'(0)$	
Analytic	*Numeric*	*Analytic*	*Numeric*	*Analytic*	*Numeric*	*Analytic*	*Numeric*
2.42659	2.42647	2.426596	2.426593	2	1.99999	2.00000	2.00000
2.90554	2.90525	2.905546	2.905530	1.09445	1.09474	1.094454	1.094470
2.90554	2.90525	2.905546	2.905530	1.09445	1.09474	1.094454	1.094470

Table 2 It is observed that the values of $\theta'(0)$ and $\emptyset'(0)$ in the present study are in conformity with those reported by Grosan and Pop, (2012), showing that the present work is validated with $Pr = 1$ and $Re = 1$.

Table 3: Skin Friction

Gr	Pr	$\tau_0 = \frac{dU}{dY}\|_{Y=0}$	$\tau_1 = \frac{dU}{dY}\|_{Y=1}$
0	0.71	79.0856	6.1993
	0.8	83.9162	6.0892
	0.9	88.9168	6.0003
	1	93.5324	5.9353
1000	0.71	2.0327	2.1526
	0.8	2.5641	2.0314
	0.9	3.1142	1.9336
	1	3.6219	1.8622

Table 3 shows the values of skin friction at the left wall and the right wall for different values of the Grashoff number to Reynolds number ratio ($\frac{Gr}{Re}$) and the Prandtl number (Pr). As Pr increases, the skin friction at both walls increases. This indicates that higher Prandtl numbers lead to higher shear stress at the walls, which is consistent with the fact that Pr represents the ratio of momentum diffusivity to thermal diffusivity.

4.0 CONCLUSION

The steady-state free convection of a nanofluid in a vertical channel was investigated and resolved analytically. Using tables and graphical representations,

DOI: https://doi.org/10.57233/ijsgs.v11i1.783 ISSNp: 2488-9229; ISSNe: 3027-1118

the behavior of several physical factors was examined. The following conclusions were reached:

i. Increasing Nr leads to a deceleration of the flow near the hot wall and an acceleration near the cold wall.
ii. As Gr increases, the velocity near the hot wall decreases, while the velocity near the cold wall increases. This behavior is due to the fact that higher Grashoff numbers indicate stronger buoyancy forces, which enhance the flow near the cold wall and reduce it near the hot wall.
iii. Near the hot wall, the velocity decreases as Pr increases and near the cold wall, the velocity increases as Pr increases. This behavior is due to the fact that higher Prandtl numbers indicate a thicker thermal boundary layer relative to the velocity boundary layer, which affects the flow dynamics.
iv. Near the hot wall, the velocity decreases as Nb increases and near the cold wall, the velocity increases as Nb increases.
v. Near the hot wall, the velocity decreases as Nt increases and near the cold wall, the velocity increases as Nt increases.
vi. As Nb increases, the temperature profile increases across the channel and as Nb increases, the nanoparticle concentration profile also increases across the channel. The concentration of nanoparticles is higher near the cold wall compared to the hot wall, reflecting the tendency of nanoparticles to move from the hot wall to the cold wall due to thermophoresis.
vii. As Nt increases, the temperature profile increases across the channel and as Nt increases, the nanoparticle concentration profile decreases across the channel. A higher Nt means that the nanoparticles are more strongly driven from the hot wall to the cold wall, which enhances the thermal conductivity of the nanofluid.
viii. As Pr increases, the temperature profile $\theta(Y)$ increases across the channel and the nanoparticle concentration profile $\emptyset(Y)$ also increases with increasing Pr.
ix. As Nb increases, the Nusselt number decreases and as Nb increases, the Sherwood number also decreases. A higher Nb leads to a thicker thermal boundary layer, which reduces the temperature gradient at the wall and more uniform distribution of nanoparticles throughout the fluid, reducing the concentration gradient at the wall, For a given Nb, the Nusselt and Sherwood numbers decrease as Nt increases.
x. As Nt increases, the Nusselt number decreases and as Nt increases, the Sherwood number increases. A higher Nt means that the nanoparticles are more strongly driven from the hot wall to the cold wall, which enhances the thermal conductivity of the nanofluid. For a given Nt, the Nusselt number decreases as Nb increases and For a given Nt, the Sherwood number decreases as Nb increases.

REFERENCE

Buongiorno, J., (2006) "Convective Transport in Nanofluids," *ASME Trans. J. Heat Transfer*, 128, pp. 240–250.

Choi, S. U. S., (1995). "Enhancing Thermal Conductivity of Fluids with Nano particles," *Development and Applications of Non-Newtonian Flows*, D. A. Siginer and H. P. Wang, eds., *ASME*, New York, MD-Vol. 231 and FED-Vol. 66, pp. 99–105.

Grosan, T., and Pop, I. (2012). Fully developed mixed convection in a vertical channel filled by a nanofluid. *Journal of Heat Transfer*, 134(8), 082501. https://doi.org/10.1115/1.4006159

Mirzaei, A., Jalili, B., Jalili, P. et al. Free convection in a square wavy porous cavity with partly magnetic field: a numerical investigation. Scientific Reports 14, 14152 (2024). https://doi.org/10.1038/s41598-024-64850-7

Murtala Sani, and I. H. Kaita. (2023). Steady State Free Convection with Heat and Mass Transfer in the Presence of Variable Thermal Conductivity . Journal of Energy Technology and Environment, 5(3). https://doi.org/10.5281/zenodo.10003527

Puspitasari, D., Pratiwi, D.K., Amran, P., Sahim, K. (2024). Steady natural convection from a vertical hot plate with variable radiation. Frontiers in Heat and Mass Transfer, 22(1), 305–315. https://doi.org/10.32604/fhmt.2023.041882

Ratha, P., K., Mishra S., R., Tripathy, R. and Pattnaik, P., K. (2022). Analytical approach on the free convection of Buongiorno model nanofluid over a shrinking surface. Proceedings of the Institution of Mechanical Engineers Part N Journal of Nanomaterials Nanoengineering and Nanosystems. 237(5):239779142211039; DOI: 10.1177/23977914221103982

Ahmad, M., Asjad, M., I., Akgül, A. and Baleanu, D. (2021) Analytical solutions for free convection flow of Casson nanofluid over an infinite vertical plate. Journal of AIMS Mathematics, 6(3): 2344-2358. doi: 10.3934/math.2021142

Jha, B., K., Sarki, M., N. (2019) Chemical reaction and Dufour effects on nonlinear free convection heat and mass transfer flow near a vertical moving porous plate. Heat Transfer—Asian Research. 1–16. https://doi.org/10.1002/htj.21649

Umar A., D., Sarki, N., M., Hamza, M., M., Dakin-Gari, S., M. and Yale, I., D. (2024). Free Convective MHD Flow of Jeffrey Fluid in a Porous Medium in the Presence of Heat Source/Sink. International Journal of Science for Global Sustainability. DOI: https://doi.org/10.57233/ijsgs.v10i1.600

Shobha K., C. and Patil M., B. (2021). Fully developed mixed convection in vertical channel filled with nanofluids with heat source or sink. Palestine Journal of Mathematics. Vol. 10 (Special Issue I) (2021), 29–38

Sarki, M., N. and Garba, N. (2024). The Impact of Heat Source/Sink on Non-Linear Free Convection Fluid Flow with Chemical Reaction. International Journal of Science for Global Sustainability. DOI: https://doi.org/10.57233/ijsgs.v10i4.745

Ajibade, O., A. and Umar M., A. (2020). Mixed convection flow in a vertical channel in the presence of wall conduction, variable thermal conductivity and viscosity. Nonlinear Engineering 2020; 9: 412–431. https://doi.org/10.1515/nleng-2020-0026

Yale, I., D., Tambuwal, B., H. and Dago, M., M. (2024). Mixed convection flow of heat generating/absorbing fluid in a vertical channel with asymmetric heating condition. *International Journal of Science for Global Sustainability*. DOI: https://doi.org/10.57233/ijsgs.v10i4.747